IOP Publishing and International Atomic Energy Agency Nuclear Fusion
Nucl. Fusion **49** (2009) 095027 (6pp) doi:10.1088/0029-5515/49/9/095027

# Investigation of electron Bernstein wave (EBW) coupling and its critical dependence on EBW collisional loss in high-$\beta$, H-mode ST plasmas

**S.J. Diem[1,a], G. Taylor[2], J.B. Caughman[1], P.C. Efthimion[2], H. Kugel[2], B.P. LeBlanc[2], C.K. Phillips[2], J. Preinhaelter[3], S.A. Sabbagh[4], J. Urban[3] and J.B. Wilgen[1]**

[1] Oak Ridge National Laboratory, Oak Ridge, TN, USA
[2] Princeton Plasma Physics Laboratory, Princeton, NJ, USA
[3] Czech Institute of Plasma Physics, Prague, Czech Republic
[4] Department of Applied Physics and Applied Mathematics, Columbia University, New York, NY, USA

E-mail: diemsj@ornl.gov

Received 30 December 2008, accepted for publication 24 July 2009
Published 4 September 2009
Online at stacks.iop.org/NF/49/095027

**Abstract**
High-$\beta$ spherical tokamak (ST) plasma conditions cut off propagation of electron cyclotron (EC) waves used for heating and current drive in conventional aspect ratio tokamaks. The electron Bernstein wave (EBW) has no density cutoff and is strongly absorbed and emitted at the EC harmonics, allowing EBWs to be used for heating and current drive in STs. However, this application requires efficient EBW coupling in the high-$\beta$, H-mode ST plasma regime. EBW emission (EBE) diagnostics and modelling have been employed on the National Spherical Torus Experiment (NSTX) to study oblique EBW to O-mode (B–X–O) coupling and propagation in H-mode plasmas. Efficient EBW coupling was measured before the L–H transition, but rapidly decayed thereafter. EBE simulations show that EBW collisional damping prior to mode conversion (MC) in the plasma scrape off reduces the coupling efficiency during the H-mode phase when the electron temperature is less than 30 eV inside the MC layer. Lithium evaporation during H-mode plasmas was successfully used to reduce this EBW collisional damping by reducing the electron density and increase the electron temperature in the plasma scrape off. Lithium conditioning increased the measured B–X–O coupling efficiency from less than 10% to 60%, consistent with EBE simulations.

**PACS numbers:** 52.35.Hr, 52.35.Qz, 52.35.Fp, 52.35.Mw

(Some figures in this article are in colour only in the electronic version)

## 1. Introduction

Tokamaks and many other magnetically confined plasma devices have utilized electron cyclotron (EC) waves to provide local electron temperature, $T_e$, measurements via EC emission (ECE) [1] as well as for localized heating via electron cyclotron resonance heating (ECRH), and current drive via electron cyclotron current drive (ECCD) [2]. However, high-$\beta$ devices, such as the spherical tokamak (ST) and reverse field pinch, routinely operate at relatively high electron densities, $n_e$, compared with the confining magnetic field, such that the plasmas are overdense, $\omega_{pe} \gg \Omega_{ce}$, where $\omega_{pe}$ is the electron plasma frequency and $\Omega_{ce}$ is the EC frequency. In these overdense devices, the propagation of EC waves beyond the plasma edge is cut off, thus prohibiting the use of ECRH or ECCD. The National Spherical Torus Experiment (NSTX [3]) routinely studies overdense plasmas with $n_e$ up to $10^{20}$ m$^{-3}$ and $B_t < 0.6$ T, so that the first four EC harmonics are overdense. An alternative to EC waves for these overdense devices is the electrostatic electron Bernstein wave (EBW) [4]. EBWs do not experience a density cutoff in the plasma, propagate mainly perpendicular to the external magnetic field until it reaches the EC resonance where the waves are strongly absorbed and emitted. However, EBWs cannot propagate outside the plasma and therefore must couple to

[a] Author to whom any correspondence should be addressed.

 

the ordinary (O) or extraordinary (X) electromagnetic modes outside the overdense region of the plasma. Coupling to the EBW can be achieved through B–X (EBW to X-mode coupling) or B–X–O (EBW to X-mode to O-mode coupling) mode conversion. The work presented here studied microwave plasma emission via B–X–O coupling on NSTX.

In the B–X–O emission process, an EBW is generated near the location where the wave frequency, $\omega$, is equal to an EC harmonic. The EBW travels radially outwards towards the plasma edge, perpendicular to the plasma magnetic field, until it encounters the upper hybrid resonance (UHR) layer where $\omega = \omega_{\mathrm{UHR}} = ((\omega_{\mathrm{pe}})^2 + (\Omega_{\mathrm{ce}})^2)^{1/2}$. At this point, the perpendicular wave number, $k_\perp$, of the EBW and slow X-mode branch are equal and full conversion between the two branches may occur provided collisional effects are negligible. The converted slow X-mode propagates back into the plasma until it encounters the left-hand cutoff of the X-mode. For particular viewing angles, the left-hand cutoff of the slow X-mode branch is coincident with the O-mode cutoff ($\omega = \omega_{\mathrm{pe}}$) and the power in the slow X-mode can be transferred efficiently to the O-mode branch. The O-mode then propagates out of the plasma and can be detected by a receiving antenna with an oblique view of the plasma. The transmission window for this process is given by [5]

$$T\left(n_\parallel, n_\perp\right) = \exp\left\{-\pi k_0 L_n \sqrt{\frac{Y}{2}}\left[2\left(1+Y\right)\left(n_{\parallel,\mathrm{opt}} - n_\parallel\right)^2 + n_\perp^2\right]\right\}, \quad (1)$$

$$Y = \frac{\Omega_{\mathrm{ce}}}{\omega}, \quad (2)$$

$$n_{\parallel,\mathrm{opt}}^2 = \frac{Y}{1+Y}. \quad (3)$$

In equation (1) above, $n_\parallel$ and $n_\perp$ are the parallel and perpendicular wave numbers, respectively, $k_0$ is the vacuum wavelength, and $L_n$ is the density scale length evaluated at the mode conversion (MC) layer. $L_n$ determines the angular width of the window. By decreasing $L_n$, the angular width of the window is increased. The centre of the B–X–O transmission window in the poloidal and toroidal angle depends on the magnetic field and its pitch angle at the MC layer. The B–X–O transmission efficiency in equation (1) only calculates the transmission at the O-mode cutoff layer and does not account for re-absorption and re-emission prior to conversion. An EBW emission (EBE) simulation code was used to calculate these losses.

The inverse process of O–X–B MC can be used to inject power into the plasma to provide localized heating and current drive (CD). The physics of B–X–O emission and O–X–B injection are reversible processes as long as $\nabla B \parallel \nabla n_{\mathrm{e}}$ [6], which is satisfied for near-midplane viewing angles used to obtain the data presented in this paper. Additionally, the introduction of radiofrequency power may excite lossy nonlinear effects such as parametric decay. Therefore, studying the B–X–O emission can be used to assess the feasibility of O–X–B coupling. Modelling has shown that adding 1 MA of off-axis EBW current drive (EBWCD) to an ST Component Test Facility (ST-CTF) plasma significantly increases plasma stability [7] and that efficient Ohkawa EBWCD can be driven well off axis [8]. However, a critical challenge for EBWCD for the ST-CTF is to establish and maintain efficient antenna coupling to the EBW in the plasma during the High confinement (H-mode) operation.

This paper presents details of EBE measurements made via B–X–O coupling during NSTX H-mode plasmas. Section 2 describes the NSTX B–X–O emission diagnostic and the EBE simulation code used to model plasma emission. Section 3 presents the EBE measurements obtained during H-mode experiments. Early low emission results (section 3.1) were determined to be caused by collisional damping of the EBW prior to MC. Edge conditioning was employed to significantly increase the EBE levels (section 3.2) allowing for an experimental mapping of the B–X–O transmission window to be performed (section 3.3). Section 4 summarizes the conclusions.

## 2. Experimental setup and EBE simulation

The EBE diagnostic on NSTX consists of two remotely steered, quadridged microwave antennas [9, 10]. The antennas are located outside the vacuum vessel, 50 cm from the plasma edge, and have an oblique view of the plasma so the diagnostic is optimized to measure the B–X–O emission. The quadridged antennas allow for a simultaneous measurement of the radiation temperature, $T_{\mathrm{rad}}$, parallel (O-mode component) and perpendicular (X-mode component) to the plasma's magnetic field when the magnetic field pitch at the MC layer is between 30° and 45°. The ratio of parallel to perpendicular components yields the polarization of the incoming radiation while the sum provides the total $T_{\mathrm{rad}}$. The system measures fundamental, second and third harmonic emission ranging from 8 to 36 GHz. Each antenna mount has two linear actuators that provide movement in the poloidal and toroidal directions between discharges; this feature allows for detailed measurements of the B–X–O transmission window. Each antenna is coupled to a dual-channel, absolutely calibrated, heterodyne radiometer system. The local oscillator for each radiometer is swept at a rate of 10 kHz to provide emission profile measurements. Results presented in this paper are from the 18–36 GHz frequency range. The optical depth for EBWs at low EC harmonic resonances is ~3000 in NSTX [11], well satisfying the blackbody condition of $\tau > 2$, so the measured $T_{\mathrm{rad}}$ can be assumed to be equal to the local $T_{\mathrm{e}}$ provided the B–X–O transmission efficiency is ~100%. For cases such that the transmission is less than 100%, EBE simulations were used to deduce the transmission efficiency.

The EBE measurements were simulated with a numerical code developed by Preinhaelter *et al* [12]. The code simulates the process of O–X–B injection; however, due to the reciprocity of the injection and emission processes [13], the absorption and emission locations are assumed to be equivalent. A bundle of 41 rays is launched in the code to simulate the measured antenna pattern of the EBE diagnostic. A full-wave code [14] calculates the transmission efficiency of the O–X–B MC assuming a 1D plasma slab model. A 3D ray-tracing code calculates the propagation and absorption of the EBW after it has mode converted. The inputs for the EBE code are the $T_{\mathrm{e}}$ and $n_{\mathrm{e}}$ profiles measured by laser Thomson scattering [15] and the magnetic equilibrium reconstructed by EFIT [16]. Collisions between electrons and ions are incorporated into the EBW dispersion relation in the

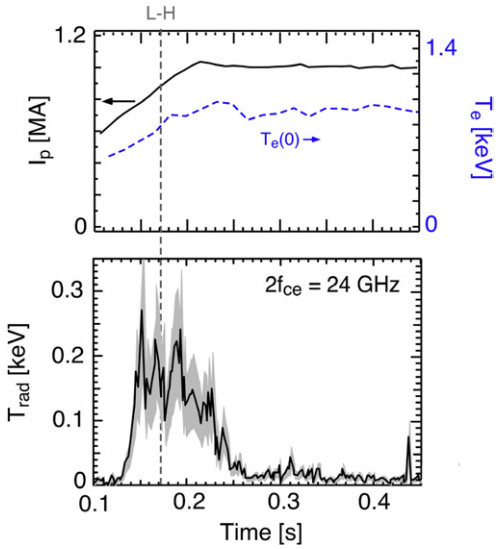


**Figure 1.** (Top) The $I_p$ (solid line) and central $T_e$ (dashed line) are shown as a function of time for an H-mode discharge. (Bottom) The time evolution of second harmonic emission at 24 GHz, from near the plasma magnetic axis, is shown for an H-mode discharge. The shaded region represents the uncertainty in the measured $T_{rad}$.

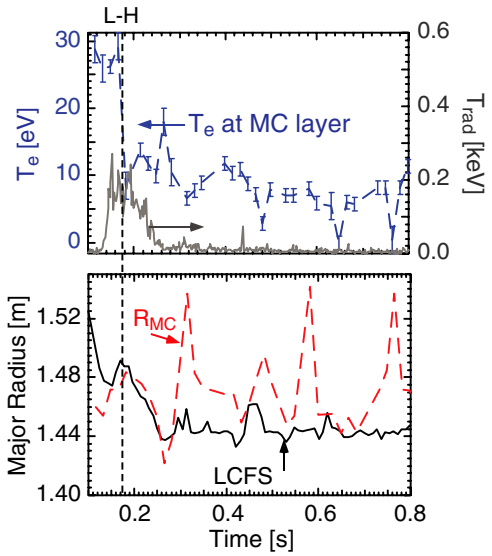


**Figure 2.** (Top) The time evolution of $T_e$ at the MC layer (dashed line) and the measured radiation temperature $T_{rad}$ (solid line) are shown. The vertical error bars represent the error in the Thomson scattering measurements. (Bottom) The time evolution of the location of the LCFS (solid line) and the position of the MC layer $R_{MC}$ (dashed line) are shown. The vertical dashed line indicates the L–H transition time.

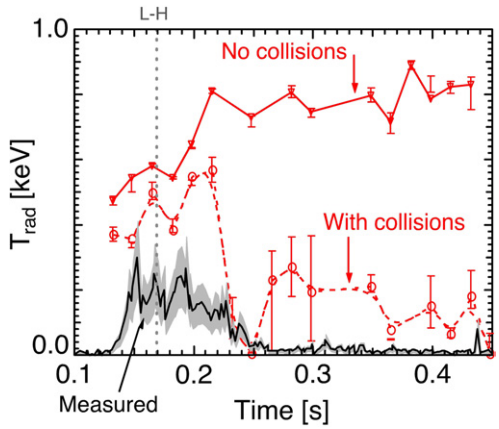


**Figure 3.** EBE simulations of the low emission H-mode data, with (dashed line) and without (solid line) collisional damping effects. The error bars represent the uncertainty in the simulations due to errors in $n_e$ and $T_e$ from Thomson scattering as well as the magnetic equilibrium reconstruction. The measured $T_{rad}$ (bottom solid line) is shown as a function of time.

EBE code with a Bhatnagar–Krook–Gross collision operator [17, 18]. The simulations neglect the effects of electron–electron collisions due to conservation of momentum while electron–neutral collisions are discarded because the neutral density is less than 5% of the $n_e$ in the vicinity of the MC layer in NSTX plasmas. The simulated effect of collisions on the EBE signal is combined with the simulated O–X–B transmission efficiency to yield the B–X–O (O–X–B) coupling efficiency that is compared with the measured EBE.

## 3. Experimental results

Good O–X–B coupling in H-mode plasmas is especially important for future STs that will routinely operate in this regime and require localized EBWCD or EBW heating (EBWH) to maintain stability at high $\beta$. Recent EBE measurements on NSTX have investigated B–X–O coupling in H-mode plasmas to assess the feasibility of establishing efficient EBW coupling.

### *3.1. Low H-mode EBE results*

Early EBE measurements in NSTX H-mode plasmas revealed very low B–X–O coupling efficiencies of less than 10% during the plasma current flattop. The characteristics of a typical H-mode plasma in NSTX, with an $I_p$ of 1 MA and central $n_e$ and $T_e$ of 4–6 $\times$ $10^{13}$ cm$^{-3}$ and 0.9 keV, respectively, are shown in figure 1. For these H-mode discharges, the measured B–X–O coupling efficiencies were 20–60% for $f_{ce}$, $2f_{ce}$ and $3f_{ce}$ (18–36 GHz) emissions during the L–H transition. However, during the H-mode phase the measured $T_{rad}$ was less than 10 eV for all measured harmonics. The emission location for second harmonic (24 GHz) emission (figure 1) remained at a constant major radius of 1 m, near the plasma magnetic axis, throughout the discharge.

Preinhaelter *et al* [12] suggested that the observed decay in EBE could be explained by collisional damping of the EBW prior to MC to the slow X-mode. Modelling suggests that EBW collisional damping becomes significant if the electron–ion collision frequency, $\upsilon_{ei}$, is greater than $10^{-4}\omega$, which typically corresponds to $T_e < 20$ at the MC layer for NSTX plasmas. For times prior to $t = 0.25$ s for the discharge shown in figure 1, the B–X–O MC layer is located within 1 cm of the last closed flux surface (LCFS) as seen in figure 2. For times greater than 0.25 s, the MC layer is shifted 3–9 cm outside the LCFS where $T_e$ is less than 10 eV (figure 2). EBE simulations of this plasma without incorporating any effects of collisional damping prior to MC (top solid line in figure 3) predict $T_{rad} \sim 0.8$ keV,

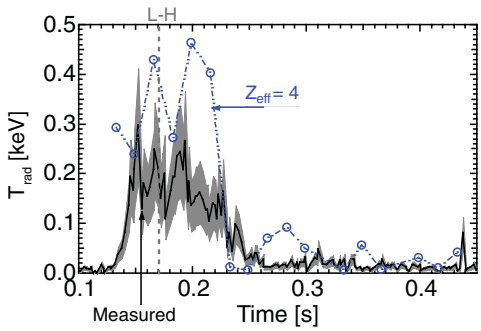


**Figure 4.** The measured $T_{rad}$ (solid line) and EBE simulations of the low emission H-mode data with collisional effects, assuming $Z_{eff} = 4$ (dot-dashed line) are shown as a function of time.

significantly higher than the measured $T_{rad}$ (bottom solid line in figure 3) which was $< 20$ eV. By including EBW collisional damping prior to MC in the EBE simulations and the measured $Z_{eff}$ from the charge exchange and recombination spectroscopy (CHERS) diagnostic on NSTX [19], the simulations predict the rapid decay in $T_{rad}$ observed in the experiment (dashed line in figure 3), but they do not reproduce the observed low $T_{rad}$ values.

In the simulation shown in figure 3, a $Z_{eff}$ value of 2 was used. This value was the closest $Z_{eff}$ measurement available from the CHERS (located 5 cm inboard from the MC layer). The $Z_{eff}$ measurement from CHERS is calculated based on the line emission from plasmas where the sole impurity is assumed to be carbon. For many of these plasmas, other impurities are present. EBE simulations with $Z_{eff}$ of 3–4 predict $T_{rad}$ levels during the H-mode phase that agree more closely with the measured results (figure 4).

The EBE simulations calculate that the ratio of $\upsilon_{ei}/\omega$ near the MC layer increased over a factor of 2 from $5 \times 10^{-5}$ at $t = 0.148$ s to $1.25 \times 10^{-4}$ at $t = 0.348$ s. The value of $\upsilon_{ei}/\omega$ after the L–H transition exceeded the simulated threshold of $\upsilon_{ei}/\omega > 10^{-4}$ for significant damping. Nearly 20–40% of the ray intensity is collisionally damped prior to the L–H transition compared with 70–90% after the transition.

The results of these early H-mode experiments and simulations suggest that by decreasing the collisionality at the MC layer, significant improvements in the power coupled from the EBW to the slow X-mode branch may be achieved. By decreasing the density in the plasma edge, the MC layer can be moved to a region of the plasma with higher temperature, thereby reducing collisional effects on EBW propagation. These results motivated the need for an edge conditioning tool to decrease $n_e$ outside the LCFS, which results in shifting the MC layer to a warmer region of the plasma. The next section discusses the method employed for edge conditioning and the resulting effects on the EBE levels.

### *3.2. H-mode EBE results with lithium conditioning*

Edge conditioning using lithium (Li) coatings on the plasma facing components has been achieved with a Li evaporation oven (LITER) [20] installed on an upper vacuum vessel port in NSTX. LITER evaporates Li onto the graphite tiles of the centre stack and lower divertor before and during a discharge. The solid Li coating pumps $D^+$ and $D^0$ by forming LiD. During

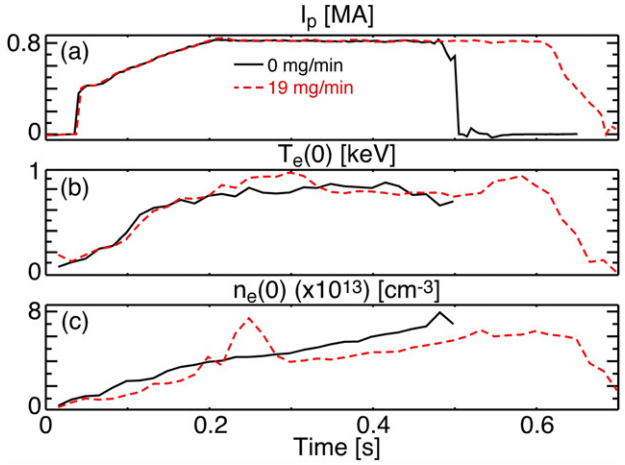


**Figure 5.** The time evolution of (*a*) $I_p$, (*b*) $T_e(0)$ and (*c*) $n_e(0)$ is shown for the target H-mode plasmas for the cases with 0 (solid line, no Li) and 19 mg min$^{-1}$ (dashed line) of evaporated Li. The L–H transition occurs at 0.145 s.

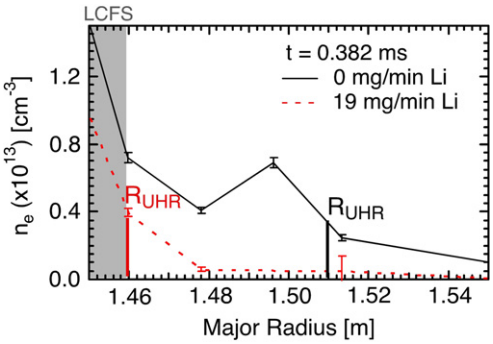


**Figure 6.** The $n_e$ profile from Thomson scattering is shown as a function of major radius in the plasma scrape off for two cases: no evaporated Li (solid line) and with 19 mg min$^{-1}$ of evaporated Li (dashed line).

a series of EBE experiments to enhance EBW coupling in H-mode discharges, the Li evaporation rate was varied from 0 to 19 mg min$^{-1}$ to observe the effect on the EBE $T_{rad}$ levels. The time evolution of major plasma parameters for the target H-mode discharge used in this study is shown in figure 5. As a result of Li edge conditioning, $n_e$ in the plasma scrape off was reduced by nearly a factor of 2 and consequently the MC layer moved from several centimetres outside the LCFS to the plasma separatrix (figure 6). By moving the MC layer closer to the plasma, $T_e$ at the fundamental MC layer during the H-mode phase increased from 5–9 eV (no Li) to nearly 20 eV (with 19 mg min$^{-1}$ of evaporated Li), as shown in figure 7.

A significant increase in the measured $T_{rad}$ from less than 50 eV to greater than 450 eV for $f_{ce} = 18$ GHz (near axis emission) was observed (figure 8(*a*)) and agreed with the EBE simulated $T_{rad}$. The measured B–X–O coupling efficiency was observed to increase from less than 10% (no Li) to 60% (with Li) as shown in figure 8(*b*). Additionally, $\upsilon_{ei}/\omega$ near the MC layer decreased by a factor of 3 from $1.2 \times 10^{-4}$ (no Li) to $4 \times 10^{-5}$ (with Li) as seen in figure 9. Consequently, the EBW ray intensity lost to collisional damping (figure 9) was reduced from 70% (no Li) to only 15% (with Li).

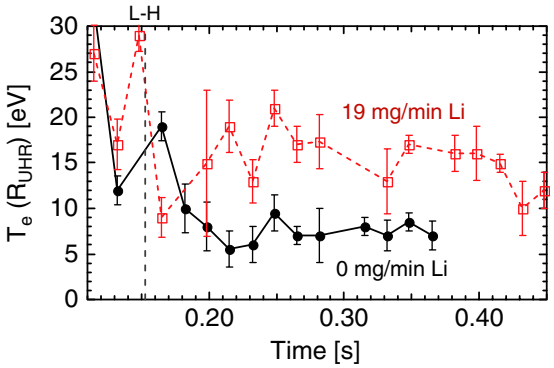


**Figure 7.** The ime evolution of $T_e$, measured by laser Thomson scattering, at the MC layer (where $\omega = \omega_{UHR}$) is shown for a plasma without Li conditioning (solid line) and with Li conditioning (dashed line). The solid vertical line indicates the L–H transition while the vertical error bars represent the uncertainty in the Thomson scattering measurement.

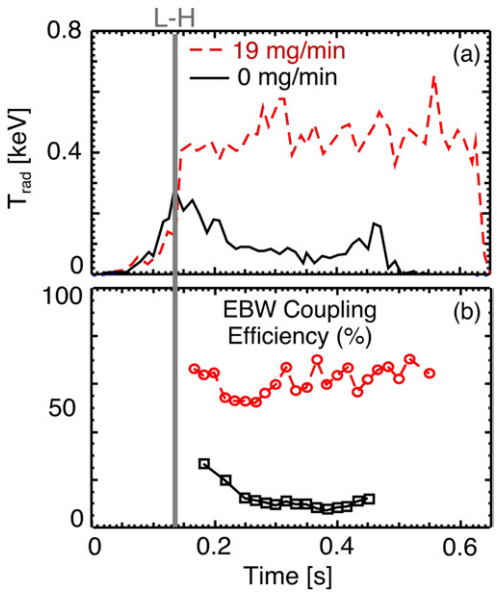


**Figure 8.** (*a*) The measured $T_{rad}$ and (*b*) B–X–O coupling efficiency are plotted for fundamental EBE (at 18 GHz) for Li evaporation rates of 0 mg min$^{-1}$ (solid line) and 19 mg min$^{-1}$ (dashed line).

The use of Li edge conditioning to increase the B–X–O coupling efficiency allowed for the development of a suitable target plasma to map the angular dependence of the B–X–O coupling efficiency window (equation (1)). The next section presents the experimental results from a mapping of the B–X–O coupling window obtained by scanning the EBW antenna viewing direction in the poloidal and toroidal directions.

### *3.3. Experimental mapping of the B–X–O coupling window*

A series of target H-mode discharges, with an $I_p = 0.9$ MA, $T_e(0) \sim 0.8$–$0.9$ keV and $n_e(0) \sim 3$–$5 \times 10^{13}$ cm$^{-3}$, were used to map the B–X–O coupling efficiency window. Li was continuously evaporated at a rate of 17 mg min$^{-1}$ during each discharge to reduce collisional losses to less than 20%, as indicated by EBE simulations. The target plasma was

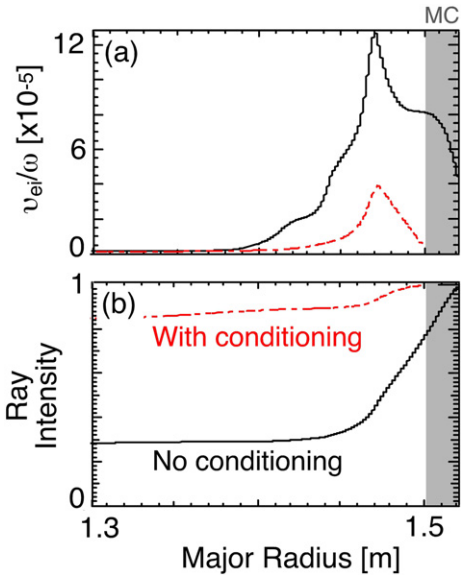


**Figure 9.** (*a*) The ratio of $\upsilon_{ei}/\omega$ and (*b*) the intensity of the central ray from EBE simulations of a plasma without Li conditioning (solid line) and one with Li conditioning (dashed line) are shown as a function of major radius. The shaded region indicates the location of the MC layer. The code results shown in this figure show details of the EBW after MC. These figures do not include the power loss due to the MC process.

repeated and the EBE diagnostic antenna was steered to a new viewing direction between discharges. The measured B–X–O coupling efficiency and predicted B–X–O transmission efficiency (equation (1)) maps for fundamental (18 GHz) and second harmonic (28 GHz), near axis emission, are shown in figure 10. The maximum measured B–X–O coupling efficiency was $62 \pm 15\%$ for the fundamental and $48 \pm 15\%$ for the second harmonic emission. Good agreement, less than 5°, between the measured and the theoretical locations (equation (1)) of the optimum angles was observed. The EBE simulation code was used to determine the poloidal and toroidal angles for optimal transmission, these angles were also within 5° of the measured value. The predicted angle location for optimal EBW transmission from both the theoretical calculations and the EBE simulations is within the 14° acceptance angle of the antenna.

## 4. Conclusion

Early H-mode experiments revealed very low B–X–O coupling efficiencies, with less than 10% coupling being observed during the $I_p$ flattop for the 18–36 GHz EBE frequency range measured. Simulations of these H-mode discharges suggested that the low emission results from significant collisional damping of the EBW prior to MC. These results motivated the need for a tool to reduce the edge collisionality in these plasmas. Lithium evaporation was used to deplete $n_e$ in the plasma scrape off, moving the MC layer to a region in the plasma where $T_e \sim 20$ eV. At these temperatures, the collisionality near the MC layer is significantly reduced, which increased the fundamental B–X–O coupling efficiency from 10% to 60%, agreeing with EBE simulation results.

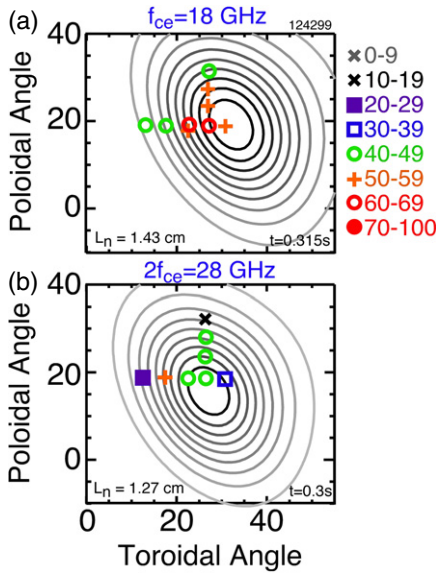


**Figure 10.** Experimentally measured B–X–O transmission efficiency map (symbols) in a Li conditioned H-mode plasma for (*a*) $f_{ce} = 18$ GHz and (*b*) $2f_{ce} = 28$ GHz. The contours represent the theoretical B–X–O transmission efficiency (equation (1)), where the centre represents 90% transmission. Subsequent contours represent a 10% decrease in transmission. The experimental measurements include effects due to the finite antenna acceptance angle of 14° and EBW collisional damping.

Similarly, the second harmonic B–X–O coupling efficiency was increased from 25% to 50%. The increase in EBE during H-mode allowed for an experimental mapping of the B–X–O coupling efficiency to be obtained. The measured, theoretically predicted (equation (1)) and simulated optimum toroidal and poloidal angles for maximum transmission in H-mode plasmas agreed within 5°, verifying that these tools can be used to determine the optimal launch angle and polarization for future EBW heating and CD systems. This work has demonstrated that using edge conditioning to raise $T_e$ at the MC layer can significantly reduce collisional losses, providing support for EBW as a viable candidate for localized heating and CD in future ST devices.

## Acknowledgments

This research was supported by USDOE DE-AC02-76CH-03073, DE-FG02-91ER-54109, DE-FG03-02ER-54684 and DE-FG02-99ER-54521 and a grant to encourage innovations in fusion diagnostic systems. The authors would like to thank L. Guttadora and P. Roney for their help in developing the NSTX EBE diagnostic.

## References

[1] Taylor G. 2007 *Fusion Sci. Technol.* **52** 119
[2] Zohm H. 2007 *Fusion Sci. Technol.* **52** 134
[3] Ono M. *et al* 2000 *Nucl. Fusion* **40** 557
[4] Bernstein I.B. 1958 *Phys. Rev.* **109** 10
[5] MjØlhus E. 1984 *J. Plasma Phys.* **31** 7
[6] Laqua H. 2007 *Plasma Phys. Control. Fusion* **49** R1–R42
[7] Peng Y.-K.M. 2005 *Plasma Phys. Control. Fusion* **47** B263
[8] Taylor G. *et al* 2004 *Phys. Plasmas* **11** 4733
[9] Diem S.J. *et al* 2006 *Rev. Sci. Instrum.* **77** 10E919
[10] Diem S.J. *et al* 2008 *Rev. Sci. Instrum.* **79** 10F101
[11] Efthimion P.C. *et al* 1999 *Rev. Sci. Instrum.* **70** 1018
[12] Preinhaelter J. *et al* 2006 *Rev. Sci. Instrum.* **77** 10F524
[13] Ram A.K. *et al* 2002 *Phys. Plasmas* **9** 409
[14] Urban J. and Preinhaelter J. 2006 *J. Plasma Phys.* **72** 1041
[15] LeBlanc B.P. *et al* 2003 *Rev. Sci. Instrum.* **74** 1659
[16] Lao L. *et al* 1985 *Nucl. Fusion* **25** 1611
[17] Bhatnagar P.L. *et al* 1954 *Phys. Rev.* **94** 511
[18] Gross E.P. and Krook M. 1956 *Phys. Rev.* **102** 593
[19] Bell R.E. *et al* 2003 $Z_{eff}$ profiles using charge exchange recombination spectroscopy on NSTX *Bull. Am. Phys. Soc.* **48** 217
[20] Kugel H.W. *et al* 2007 *J. Nucl. Mater.* **363–365** 791